Crimson Publishers
Wings to the Research

Research Article

Establishing the Constitutive Equations during Hot Tensile Deformation in an Mg-Zn-Y-Ca-Zr Alloy Fabricated by Multidirectional Forging and Rolling

Furong Cao[1,2]* and Renjie Liu[1]

[1]School of Materials Science and Engineering, China

[2]State Key Laboratory of Rolling and Automation, China

ISSN: 2643-7066

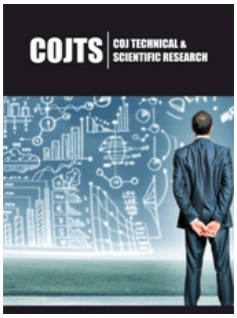

***Corresponding author:** Furong Cao, School of Materials Science and Engineering, State Key Laboratory of Rolling and Automation, Northeastern University, Shenyang, China

Submission: February 24, 2023

Published: March 10, 2023

Volume 4 - Issue 2

How to cite this article: Furong Cao and Renjie Liu. Establishing the Constitutive Equations during Hot Tensile Deformation in an Mg-Zn-Y-Ca-Zr Alloy Fabricated by Multidirectional Forging and Rolling. COJ Tech Sci Res. 4(2). COJTS. 000583. 2023. DOI: 10.31031/COJTS.2023.04.000583

Abstract

To establish constitutive equations for the implementation of load determination and numerical simulation, a new Mg-2.70Zn-1.34Y-0.37Ca-0.02Zr magnesium alloy has been fabricated by multidirectional forging and hot rolling, and its true stress-true strain curves were obtained at elevated temperatures and different strain rates. The flow stress curves at 723K and lower strain rates exhibit a slow strain hardening stage, followed by a strain softening stage. Except for this, other flow stress curves behave like conventional single peak curves. An Arrhenius constitutive equation was established. The determination coefficient was 0.978, the ratio of predicted stress to experimental stress was 0.961, and the average absolute relative error was 2.1%, indicative of high accuracy of the hyperbolic sine law. A modified Fields-Backofen constitutive equation was established. The determination coefficient was 0.924, and the ratio of prediction stress to experimental stress was 0.987, indicative of high prediction precision.

Keywords: Mg-Zn-Y alloy; Multidirectional forging; Rolling; Hot tension; Flow stress; Constitutive equation

Introduction

Because of high modulus-to-density ratio, good specific strength, and damping performance, Mg-Zn-Y magnesium alloys have the potential for application in automobile manufacture, aerospace industry, and so forth [1-4]. Hence, a new Mg-3Zn-1Y-0.5Ca-0.5Zr (hereinafter denoted as ZWCK3100) alloy is designed. Owing to limited slip systems of magnesium at room temperature, von Mises deformation compatibility of five independent slip systems cannot be met in magnesium alloy. Thus, plastic forming of magnesium alloy such as Mg-Zn-Y magnesium alloys with a high Zn and Y content is difficult at room temperature. However, hot deformation like hot compression and hot tension can initiate the non-basal etc. slip systems and improve the plasticity of magnesium alloys like Mg-Zn-Y alloys at elevated temperature [5-9]. Thus, it is necessary to investigate the hot tensile deformation behavior of ZWCK3100 alloy. Multidirectional Forging (MDF), as a severe plastic deformation method and because of its suitable large-scale billet fabrication, has been investigated in magnesium alloys [10-14] except Mg-Zn-Y alloys, but little report is available reporting MDF of Mg-Zn-Y alloy. Meanwhile, conventional rolling has the advantage of mass production due to its high rolling speed. As per our literature survey, little work is available about combination of MDF and hot rolling to produce ZWCK3100 alloy. Thus, it is necessary to fabricate ZWCK3100 alloy plate and investigate its high temperature deformation behavior.

Constitutive modeling is an interesting topic during hot deformation, and is a prerequisite for the implementation of numerical simulation and calculation of deformation load. Constitutive modeling can be classified as phenomenological equation, physics-based constitutive equation, and Artificial Neural Network (ANN) model [15]. Due to their higher

correlation coefficients and lower absolute relative errors, the phenomenological equations such as Arrhenius constitutive equation [5,6], modified Johnson-Cook constitutive equation [16], and modified Zerilli-Armstrong constitutive equation [17] in magnesium alloys were established. According to our survey, little work is reported on modeling an Arrhenius constitutive equation and a modified Fields-Backofen constitutive equation in ZWCK3100 magnesium alloy. To the best of authors' knowledge, there is no report studying the Arrhenius constitutive equation and modified Fields-Backofen constitutive equation in the present alloy. Thus, it is necessary to establish both equations. In the present work, our research aims include three aspects:

(i) To fabricate a new ZWCK3100 alloy using MDF and hot rolling

(ii) To obtain the flow stress curves at elevated temperatures

(iii) To construct an Arrhenius constitutive equation and a modified Fields-Backofen constitutive equation in this alloy.

Experimental Process

Pure Zn, pure Mg raw materials, Mg-30Y, Mg-30Ca, and Mg-30Zr mater alloys were melted at 993K in an electric resistance furnace with the protection of RJ-5 flux and argon atmosphere. The analyzed alloy composition was Mg-2.70Zn-1.34Y-0.37Ca-0.02Zr (mass.%). After the melt was stirred and held for 5min, the melt was solidified into an ingot in an internally water-cooled copper crucible. After being homogenized at 673K for 14h, the ingot surface was milled to remove the cast defects. Then the milled ingot was machined by spark discharge processing into cuboid billets. The dimension of the cuboid billet was 40mm×30mm×20mm. Then MDF and rolling started. The schematic diagram of MDF and rolling was shown elsewhere [18]. The forging temperature was 673K, and the holding time during intermediate forging was 30min. The pass strain was 0.288. Then, after heated at 673K for 1h, the billet was hot rolled at 673K from 20mm thickness to 16.73mm thickness for four passes. The pass reductions were 8%, 7%, 6%, and 5.5%, respectively. The samples for tensile testing were machined along the rolling direction from above-mentioned billets and plates. The dimension of the sample for high temperature tensile test was 6mm×3mm×2mm. After annealed at 673K for 60min and held at designated testing temperatures for 15min, the tensile tests were performed on a Shimidazu- AG-Xplus 100kN tester in the temperature range of 573~723K and strain rate range of 1.67×10^{-2}~$1.67\times10^{-4}s^{-1}$.

Results and Discussion

Flow stress curves at elevated temperatures

(Figure 1) presents the flow stress curves of ZWCK3100 alloy at different temperatures and initial strain rates. The flow stress curves at 723K and lower strain rates exhibit a slow strain hardening stage, followed by a strain softening stage, which indicates the occurrence of dynamic grain growth. Except for this, other flow stress curves behaves like conventional single peak curves, indicating the occurrence of dynamic recrystallization.

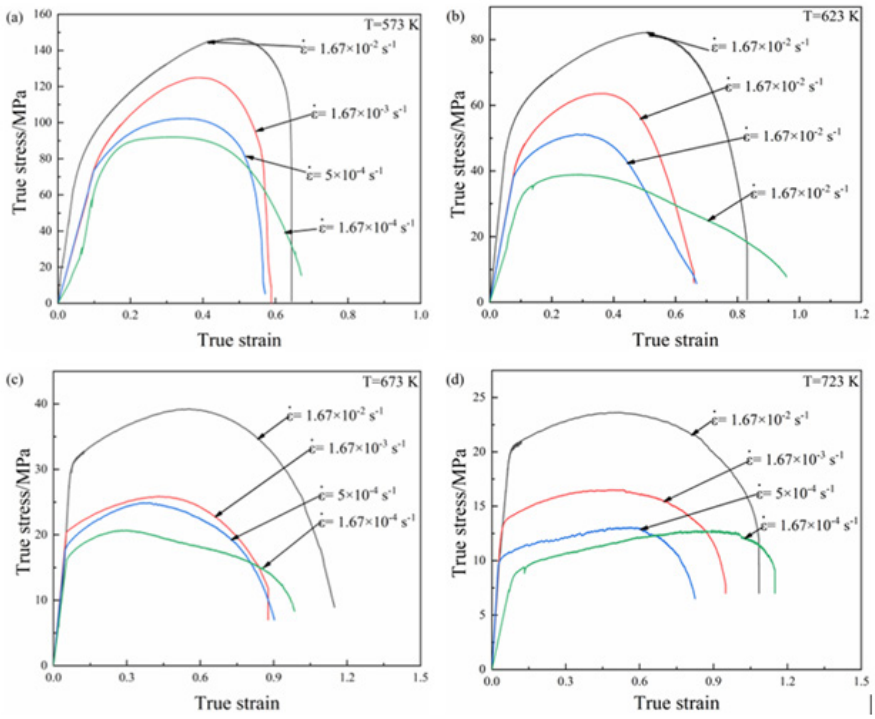

Figure 1: Flow stress curves of ZWCK3100 alloy at different temperatures and initial strain rates: a) 573K b) 623K c) 673K d) 723K.

Hyperbolic sine Arrhenius equation

The $\sigma-\dot{\varepsilon}$ relationship in the Arrhenius equation is expressed as

$$\dot{\varepsilon}=A_1\sigma^{(n_1)},\alpha\sigma<0.8 \quad (1)$$

$$\dot{\varepsilon}=A_2\exp(\beta\sigma),\alpha\sigma<1.2 \quad (2)$$

where $\sigma-\dot{\varepsilon}$ means the stress-strain rate, and A_1,n_1,A_2 and β are material constants.

Arrhenius equation can be expressed as [19]

$$\dot{\varepsilon}=A[\sinh(\alpha\sigma)]^n\exp(\frac{-Q}{RT}) \quad (3)$$

where A is the material constant, and α is the stress amplifier factor, n is the stress exponent, Q is the activation energy for deformation, J/mol, R is the universal gas constant, 8.314 $J\cdot K^{-1}\cdot mol^{-1}$, and *T* is the absolute temperature, K, here $\alpha=\beta/n_1$.

Zener–Holloman parameter is given by [20]

$$Z=\dot{\varepsilon}\exp(\frac{Q}{RT})=A[\sinh(\alpha\sigma)]^n \quad (4)$$

Logarithm is taken on equations (1),(2), and (3), one obtains.

$$\ln\dot{\varepsilon}=\ln A_1+n_1\ln\sigma \quad (5)$$

$$\ln\dot{\varepsilon}=\ln A_2+\beta\sigma \quad (6)$$

$$\ln\dot{\varepsilon}=n\ln[\sinh(\alpha\sigma)]+\ln A(\frac{-Q}{RT}) \quad (7)$$

It follows from equations (5)-(7) that n_1 is the slope of $\ln\dot{\varepsilon}$-$\ln\beta$ curve, β is the slope of $\ln\dot{\varepsilon}-\sigma$ curve, and *n* is the slope of $\ln\dot{\varepsilon}=\ln[\sinh(\alpha\sigma)]$ as shown in (Figure 2). (Figures 2a-2d) presents the linear fit diagram of $\ln\sigma-\ln\dot{\varepsilon},\sigma-\ln\dot{\varepsilon},\ln[\sinh(\alpha\sigma)]-\ln\dot{\varepsilon}$ and $\ln[\sinh(\alpha\sigma)]-1000/T$, respectively. The slope of each strain line represents different material constant values. As shown in (Figure 2a), n_1 values are 6.088, 6.798, 7.166, and 9.387, respectively. As shown in (Figure 2b), β values are 0.080, 0.106, 0.238, and 0.382, respectively.

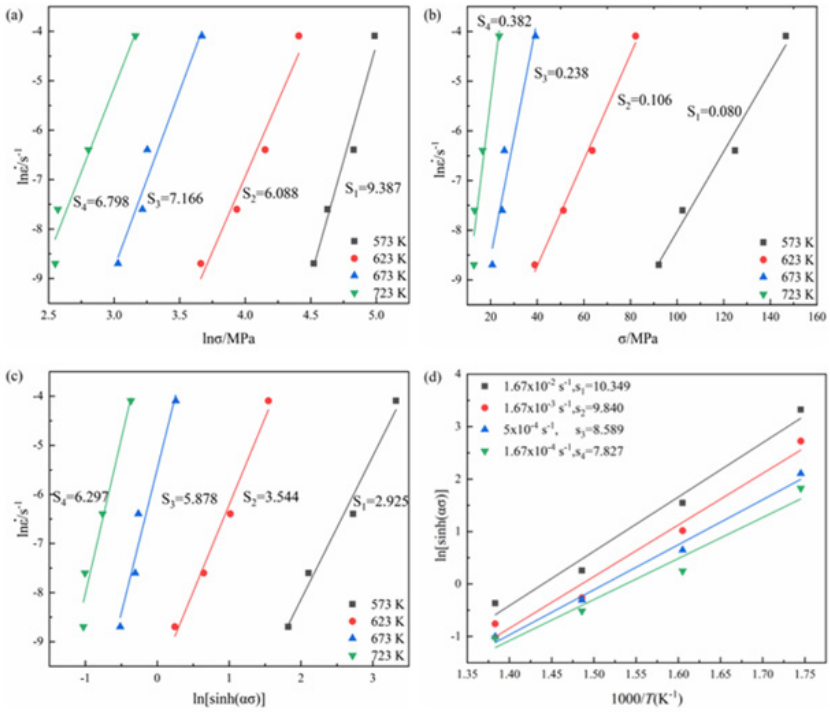

Figure 2: Relational curves under different deformation conditions
a) $\ln\sigma-\ln\dot{\varepsilon}$ b) $\sigma-\ln\dot{\varepsilon}$ c) $\ln[\sinh(\alpha\sigma)]-\ln\dot{\varepsilon}$ d) $\ln[\sinh(\alpha\sigma)]-1000/T$ Si(i=1,2,3,4) denotes the slope

Hence, average n_1 is obtained. n_1 =7.360. Average β is obtained, β=0.2015. Thus, α=β/n1=0.027. (Table 1) shows the peak stresses (MPa) of ZWCK3100 alloy under different deformation conditions.

Q formula is expressed as

$$Q=R\left[\frac{\partial\ln[\sinh(\alpha\sigma)]}{\partial(\frac{1}{T})}\right]_{\dot{\varepsilon}}\left[\frac{\partial\ln\dot{\varepsilon}}{\partial\ln[\sinh(\alpha\sigma)]}\right]_T$$

$$=Rn\left[\frac{\partial\ln\dot{\varepsilon}}{\partial\ln[\sinh(\alpha\sigma)]}\right]_T \quad (8)$$

Table 1: The peak stresses (MPa) of ZWCK3100 alloy under different deformation conditions.

T/K	$\dot{\varepsilon}$/s−1			
	1.67×10^{-2}	1.67×10^{-3}	5×10^{-4}	1.67×10^{-4}
573	146.672	124.883	102.351	92.154
623	82.221	63.593	51.202	38.903
673	39.223	25.871	24.923	20.702
723	23.622	16.522	13.084	12.801

Let

$$p=\left[\frac{\partial \ln \dot{\varepsilon}}{\partial \ln[\sinh(\alpha\sigma)]}\right]_T \quad (9)$$

(Figure 2d) is the linear fitting of $\ln\left[\sinh\left(\alpha\sigma\right)\right]-1000/T$. Its slope is p. Hence, as per equations (8) and (9), one gets $Q=R\times n\times p$. Thus, Q values under different conditions can be obtained, as shown in (Table 2). The average activation energy for deformation is 354.625kJ/mol. Substitution of Q values and other relevant parameters into equation (4), lnZ is obtained (Table 3) shows the lnZ values of ZWCK3100 alloy under different deformation conditions.

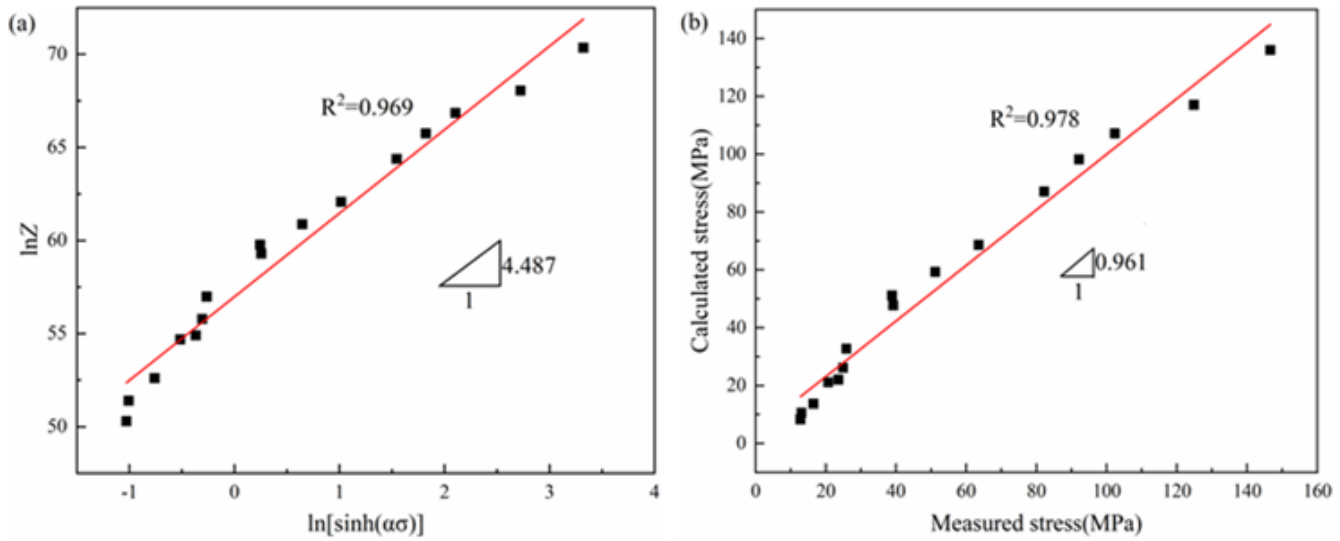

Figure 3: Fitting line of ZWCK3100 alloy
a)lnZ- ln[sinh(ασ)] b)Comparison of predicted stress and experimental stress

Table 2: Deformation activation energy of ZWCK3100 alloy under different deformation conditions: kJ/mol.

T/K	$\dot{\varepsilon}$/s−1			
	1.67×10^{-2}	1.67×10^{-3}	5×10^{-4}	1.67×10^{-4}
573	251.672	239.294	208.871	190.341
623	304.931	289.934	253.073	230.621
673	505.752	480.878	419.742	382.503
723	541.804	515.156	449.662	409.769

Table 3: lnZ values of ZWCK3100 alloy under different deformation conditions.

T/K	$\dot{\varepsilon}$/s−1			
	1.67×10-2	1.67×10-3	5×10-4	1.67×10-4
573	70.347	68.045	66.839	65.742
623	64.373	62.071	60.865	59.768
673	59.287	56.984	55.778	54.681
723	54.903	52.601	51.395	50.298

(Figure 3a) shows the linear fit curve of $\ln Z-\ln\left[\sinh\left(\alpha\sigma\right)\right]$. The slope is stress exponent *n*, and the intercept is lnA. Hence, n=4.487. lnA=56.975, hence $A=5.545\times10^{24}$. (Figure 3b) presents the comparison of predicted stress and experimental stress. The determination coefficient, R^2, is 0.978, and the slope is 0.961, very close to 1, which indicates that such a model is excellent.

Above-mentioned data is substituted into equation (3) gives

$$\dot{\varepsilon}=5.545\times10^{24}[sinh(0.027\sigma)]^{4.487} exp(\frac{-354625.2}{RT})(10)$$

Z can be expressed as

$$Z=\dot{\varepsilon}\,exp(\frac{354625.2}{RT})= 5.545\times10^{24}[sinh(0.027\sigma)]^{4.487}\,(11)$$

As per equations (10) and (11), the flow stress in Arrhenius equation can be obtained.

$$\sigma_A = \left(\frac{1}{0.027}\right)\left\{\ln\left(\frac{Z}{5.545\times10^{24}}\right)^{\left(\frac{1}{4.487}\right)} + \left[\left(\frac{Z}{5.545\times10^{24}}\right)^{\left(\frac{2}{4.487}\right)}+1\right]^{\frac{1}{2}}\right\} \quad (12)$$

(Figure 3b) presents the comparison result of predicted stress and experimental stress. The determination coefficient was 0.978, the ratio of prediction stress to experimental stress was 0.961, indicative of excellent agreement. To validate the accuracy of Arrhenius equation, Average Absolute Relative Error (AARE) is used to characterize the prediction capability of the model:

$$AARE(\%) = \frac{1}{N}\sum_{i=1}^{N}\sqrt{\left(\frac{E_i - P_i}{E_i}\right)^2} \quad (13)$$

where N-number of stress value, E_i – experimental stress, and P_i – predicted stress. Thus, AARE=2.1%, indicative of excellent fitting effect.

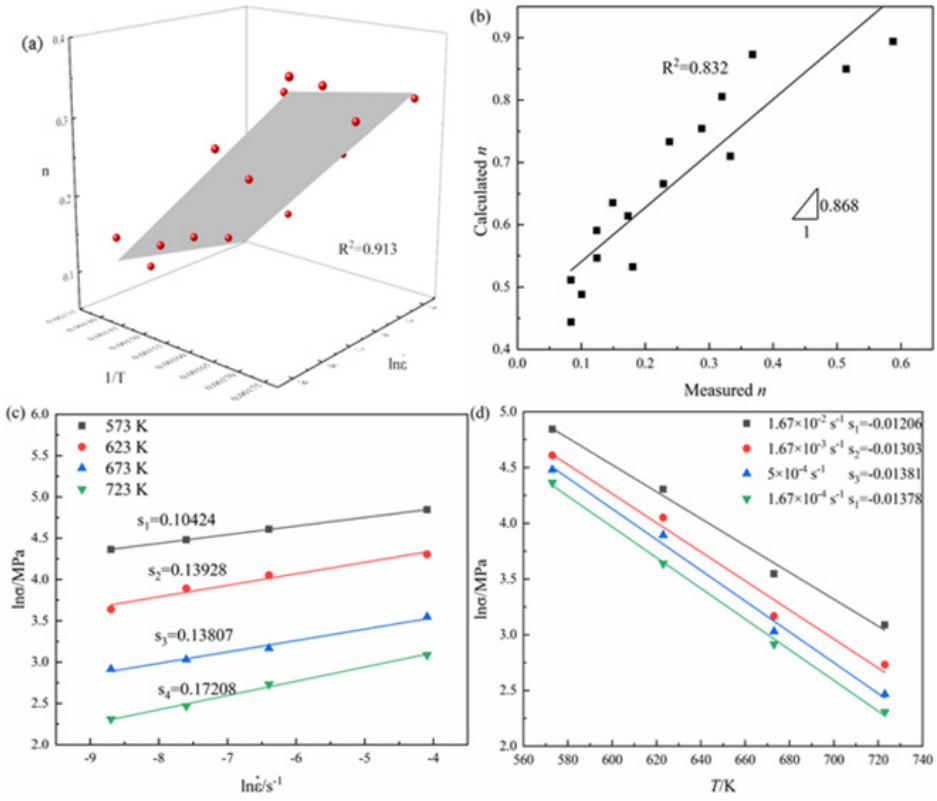

Figure 4: The relation curves between different parameters
a)n-value under different conditions b)fitting curve between predicted n-value and experimental n-value c)m-value under different conditions d)relation curve of lnσ-T.

Modified Fields-Backofen constitutive equation

Fields-Backofen constitutive equation is given by the following [21]

$$\sigma = K\varepsilon^n \dot{\varepsilon}^m \quad (14)$$

where K—hardening coefficient; n—strain-hardening exponent; m—strain ratesensitivity index. Fields-Backofen equation describes well the strain-hardening process, but in consideration of the softening stage in the flow stress curves, a modified Fields-Backofen equation considering the softening stage is required and given by [22]

$$\sigma = K\varepsilon^n \dot{\varepsilon}^m \exp(bT + s\varepsilon) \quad (15)$$

where b —softening ratio; s —softening parameter. Logarithm is taken on equation (15), one obtains the following:

$$\ln\sigma = \ln K + n\ln\varepsilon + m\ln\dot{\varepsilon} + bT + s\varepsilon \quad (16)$$

Relevant parameters can be obtained according to the relationship between $\ln\sigma$, $\ln\varepsilon$, $\ln\dot{\varepsilon}$ and T.

Strain-hardening exponent n-value: As shown in (Table 4), n-values can be obtained as per the relationship between $\ln\sigma$ and $\ln\varepsilon$, n-values are fitted with 1/T and $\ln\dot{\varepsilon}$, one gets formula (17)

$$n = -0.97863 - 0.00968\ln\dot{\varepsilon} + 725.52018/T \quad (17)$$

The experimental parameters are substituted into above formula, the predicted n-values are shown in (Table 5). The fitting effect is shown in (Figures 4a & 4b). The determination coefficient is 0.832, and the slope is 0.868, indicative of good fitting.

Table 4: The n-values of ZWCK3100 alloy under different deformation conditions

T(K)	$\dot{\varepsilon}$(s−1)			
	1.67×10^{-2}	1.67×10^{-3}	5×10^{-4}	1.67×10^{-4}
573	0.32	0.514	0.368	0.588
623	0.228	0.333	0.238	0.288
673	0.125	0.124	0.173	0.149
723	0.084	0.101	0.084	0.18

Table 5: The predicted n-values of ZWCK3100 alloy under different deformation conditions.

T(K)	$\dot{\varepsilon}$(s−1)			
	1.67×10^{-2}	1.67×10^{-3}	5×10^{-4}	1.67×10^{-4}
573	0.805	0.666	0.546	0.444
623	0.85	0.71	0.591	0.488
673	0.873	0.733	0.614	0.511
723	0.894	0.754	0.635	0.532

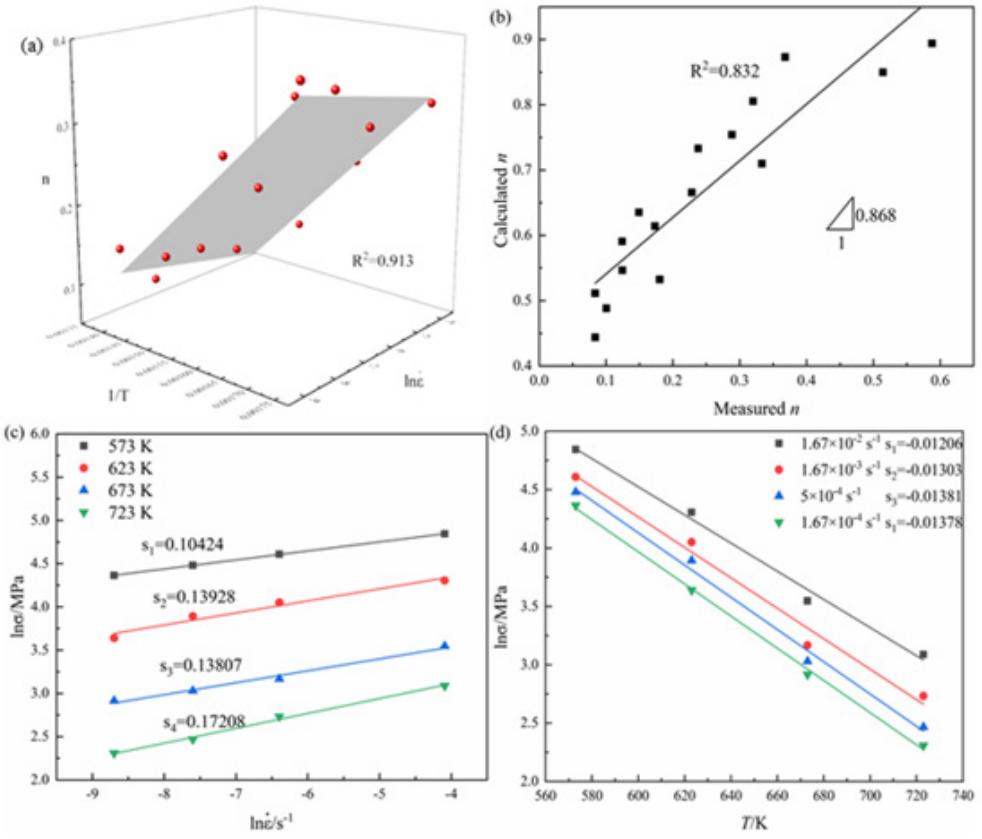

Figure 4: The relation curves between different parameters
a)n-value under different conditions b)fitting curve between predicted n-value and experimental n-value c)m-value under different conditions d)relation curve of lnσ-T.

Strain rate sensitivity index-m-value: As per (Figure 4c), the fitted formula of m-values at different temperatures is shown in equation (18):

$$m = -0.12378 + 0.00040T \quad (18)$$

Softening ratio b: As is shown in (Figure 4d), at four experimental strain rates, the softening ratios of this alloy are -0.01206, -0.01303, -0.01381 and -0.01378, respectively. The mean value is b-value, b=-0.01317.

Softening parameter s: Presuming that $\ln K + m\ln\dot{\varepsilon} + bT$ is K_1 at given temperature and strain rate, when $\varepsilon=e^{-1.5}$ and $\varepsilon=e^{-2}$, equation (15) is simplified as:

$$\ln\sigma_{e^{-1.5}} = n\ln e^{-1.5} + se^{-1.5} + K_1 \quad (19)$$

$$\ln\sigma_{e^{-2}} = n\ln e^{-2} + se^{-2} + K_1 \quad (20)$$

After equation (19) subtracts equation (20), one obtains

$$s = \frac{\ln(\frac{\sigma_{e^{-1.5}}}{\sigma_{e^{-2}}}) - 0.5n}{0.08779} \quad (21)$$

Substitution of experimental data into above equation, s values under different conditions are obtained. s values are fitted with 1/T and $\ln\dot{\varepsilon}$, one gets (Figure 5a). The determination coefficient of comparing predicted value and experimental values is 0.950 with good fitting effect. Hence, equation (22) is obtained:

$$s = -13.095 + 13598.869\frac{1}{T} - 1.191\ln\dot{\varepsilon} - 1.974\times10^{9}\frac{1}{T^3} - 0.0015(\ln\dot{\varepsilon})^3 + 1021.602\frac{\ln\dot{\varepsilon}}{T} \quad (22)$$

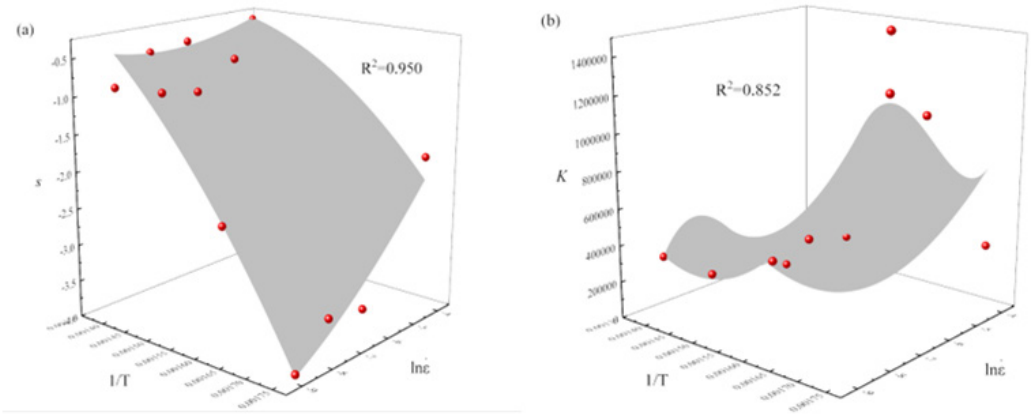

Figure 5: The relation curves between different parameters a)s as a function of 1/T and $\ln\dot{\varepsilon}$ b)K as a function of 1/T and $\ln\dot{\varepsilon}$

Hardening parameter K: As shown in (Figure 5b), the relation curves of K as a function of 1/T and $\ln\dot{\varepsilon}$. The determination coefficient is 0.852 with good fitting effect. Thus, equation (23) is obtained

$$K = 2.783\times10^{7} - 2.997\times10^{10}\frac{1}{T} + 3.346\times10^{6}\ln\dot{\varepsilon} + 1.030\times10^{13}\frac{1}{T^{2}} + 5.846\times10^{5}(\ln\dot{\varepsilon})^{2} + 3.172\times10^{4}(\ln\dot{\varepsilon})^{3} \quad (23)$$

Aforementioned parameters are substituted into equation (15), a modified Fields-Backofen constitutive equation was established as follows:

$$\sigma = K\varepsilon^{n}\dot{\varepsilon}^{m}\exp(bT + s\varepsilon)$$

$$K = 2.783\times10^{7} - 2.997\times10^{10}\frac{1}{T} + 3.346\times10^{6}\ln\dot{\varepsilon} + 1.030\times10^{13}\frac{1}{T^{2}} + 5.846\times10^{5}(\ln\dot{\varepsilon})^{2} + 3.172\times10^{4}(\ln\dot{\varepsilon})^{3}$$

$$n = -0.97863 - 0.00968\ln\dot{\varepsilon} + 725.52018/T$$

$$m = -0.12378 + 0.00040T$$

$$b = -0.01317$$

$$s = -13.095 + 13598.869\frac{1}{T} - 1.191\ln\dot{\varepsilon} - 1.974\times10^{9}\frac{1}{T^{3}} - 0.0015(\ln\dot{\varepsilon})^{3} + 1021.602\frac{\ln\dot{\varepsilon}}{T}$$

Validation of predicted stress and experimental stress using established Fields-Backofen equation: Substitution of experimental parameters into above-mentioned formula, the predicted stresses can be obtained. (Figure 6) presents the validation curve between predicted stresses and experimental stresses. The determination coefficient is 0.924, and the fitting slope is 0.987, which indicate that the predicted flow stress is slightly lower than the experimental stress.

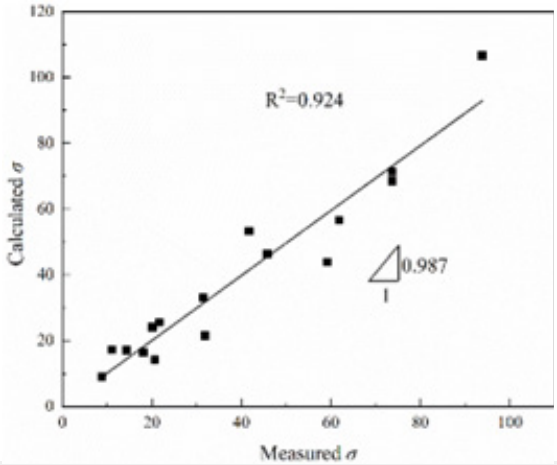

Figure 6: Validation curve between predicted stress and experimental stress

Conclusion

(i) The flow stress curves at 723K and lower strain rates exhibit a slow strain hardening stage, followed by a strain softening stage. Except for this, other flow stress curves behave like conventional single peak curves.

(ii) An Arrhenius constitutive equation was established:

$$\dot{\varepsilon} = 5.545\times10^{24}[sinh(0.027\sigma)]^{4.487} exp(\frac{-354625.2}{RT})$$

The determination coefficient was 0.978, the ratio of predicted stress to experimental stress was 0.961, and the average absolute relative error was 2.1%, implying high accuracy of the hyperbolic sine law.

(iii) A modified Fields-Backofen constitutive equation was established:

$$\sigma = K\varepsilon^{n}\dot{\varepsilon}^{m} exp(bT+s\varepsilon)$$

$$K = 2.783\times10^{7} - 2.997\times10^{10}\frac{1}{T} +3.346\times10^{6} ln\dot{\varepsilon} + 1.030\times10^{13}\frac{1}{T^{2}} +5.846\times10^{5}(ln\dot{\varepsilon})^{2} + 3.172\times10^{4}(ln\dot{\varepsilon})^{3}$$

$$n = -0.97863 - 0.00968\ln\dot{\varepsilon} + 725.52018/T$$

$$m = -0.12378 + 0.00040T$$

$$b = -0.01317$$

$$s = -13.095 + 13598.869\frac{1}{T} - 1.191ln\dot{\varepsilon} - 1.974\times10^{9}\frac{1}{T^{3}} - 0.0015(ln\dot{\varepsilon})^{3} + 1021.602\frac{ln\dot{\varepsilon}}{T}$$

The determination coefficient was 0.924, and the ratio of prediction stress to experimental stress was 0.987, indicative of high precision.

References

1. Dai S, Wang F, Wang Z, Liu Z, Mao PL (2020) Microstructure, mechanical properties, and texture evolution of Mg-Zn-Y-Zr alloy fabricated by hot extrusion-shearing process. J Mater Sci 55: 375-388.
2. Hao JQ, Zhang JS, Li BQ, Xie RZ (2021) Effects of 14H LPSO phase on the dynamic recrystallization and work hardening behaviors of an extruded Mg-Zn-Y-Mn alloy. Mater Sci Eng A 804: 140727.
3. Bazhenov VE, Saidov SS, Tselovalink Yu V, Voropaeva OO, Plisetskaya IV, et al. (2021) Comparison of castability, mechanical, and corrosion properties of Mg-Zn-Y-Zr alloys containing LPSO and W phases. Trans Nonferrous Met Soc China 31:1276-1290.
4. Dong XR, Yu H, Kang SM, Yu W, Jiang BA, et al. (2021) A comparable study of $Mg_{98.15}Y_{1}Zn_{0.85}$ sheets fabricated by twin-roll casting and direct-chill casting and related annealing behavior. Mater Sci Eng A 815:141316.
5. Kwak TY, Lim HK, Kim WJ (2017) Effect of the volume fraction of the icosahedral phase on the microstructures, hot compressive behaviors and processing maps of Mg-Zn-Y alloys. J Alloys Compd 725: 711-723.
6. Gao FY, Yang LW, Fan ZB, Lin XP, Yang YS, et al. (2022) Effects of morphology and I-$Mg_{3}Zn_{6}Y$ second-phase distribution on hot-compressive-deformation behavior of Mg-Zn-Y-Zr alloy under a strain rate of $1.0s^{-1}$. Mater Sci Eng A 834: 142556.
7. Hao JQ, Zhang JS, Gong XY, Li BQ (2021) Hot deformation behavior and workfability of the homogenized Mg-5.8Zn-1.2Y-1Mn alloy containing I and W phases. J Mater Res Technol 15: 2202-2212.
8. Li LH, Qi FG, Wang Q, Hou CH, Zhao N, et al. (2020) Hot deformation behavior of $Mg_{95.21}Zn_{1.44}Y_{2.86}Mn_{0.49}$ alloy containing LPSO phase. Mater Charact 169: 110649.
9. Fata A, Faraji G, Mashhadi MM, Tavakkoli V (2016) Hot tensile deformation and fracture behavior of ultrafine-grained AZ31 magnesium alloy processed by severe plastic deformation. Mater Sci Eng A 674: 9-17.
10. Mehrabi A, Mahmudi R, Miura H (2019) Superplasticity in a multi-directionally forged Mg-Li-Zn alloy. Mater Sci Eng A 765:138274.
11. Azizi A, Mahmudi R (2019) Superplasticity of fine-grained Mg-xGd alloys processed by multi-directional forging. Mater Sci Eng A 767: 138436.
12. Li JL, Wu D, Yang QB, Chen RS (2016) Superplasticity of multi-directional impact forged Mg-Gd-Y-Zr alloy. J Alloys Compd 672: 27-35.
13. Kandalam S, Sabat RK, Bibhanshu N, Avadhani GS, Kumar S, et al. (2017) Superplasticity in high temperature magnesium alloy WE43. Mater Sci Eng A 687: 85-92.
14. Miura H, Minami K, Kobayashi M, Watanabe C (2021) Multi-directional forging and warm extrusion of AZ80Mg Alloys. Mater Trans 62: 610-619.
15. Lin YC, Chen XM (2011) A critical review of experimental results and constitutive descriptions for metals and alloys in hot working. Mater Des 32: 1733-1759.
16. Cao FR, Sun CF, Liu SY, Liang JR, Liu RJ, et al. (2022) Microstructures, hot tensile deformation behavior and constitutive modeling in a superlight Mg-2.76Li-3Al-2.6Zn-0.39Y alloy. J Alloys Compd 896: 163049.
17. Cao FR, Guo HZ, Guo NP, Kong ST, Liang JR (2023) Room-temperature strengthening, portevin-le chatelier effect, high-temperature tensile deformation behavior, and constitutive modeling in a lightweight Mg-Gd-Al-Zn Alloy. Mater 16(4): 1639.
18. Cao FR, Zhang J, Ding X, Xue GQ, Liu SY, et al. (2019) Mechanical properties and microstructural evolution in a superlight Mg-6.4Li-3.6Zn-0.37Al-0.36Y alloy processed by multidirectional forging and rolling. Mater Sci Eng A 760: 377-393.
19. Mirzadeh H (2019) Developing constitutive equations of flow stress for hot deformation of AZ31 magnesium alloy under compression, torsion, and tension. Int J Mater Form 12:643-648.
20. Zener C, Hollomon JH (1944) Effect of strain rate upon plastic flow of steel. J Appl Phys 15: 22-32.
21. Fields DS, Backofen WA (1957) Determination of Strain Hardening Characteristics by Torsion Testing. Proc ASTM 57: 1259-1272.
22. Ji GL, Li L, Qin FL, Zhu LY, Li Q (2017) Comparative study of phenomenological constitutive equations for an as-rolled M50NiL steel during hot deformation. J Alloys Compd 695: 2389-2399.